Operating Cost Comparison of a Single-Stack and a Multi-Stack Hybrid Fuel Cell Vehicle through an Online Hierarchical Strategy

Mohammadreza Moghadari, *Student Member, IEEE*, Mohsen Kandidayeni, *Member, IEEE*, Loïc Boulon, *Senior Member, IEEE*, and Hicham Chaoui, *Senior Member, IEEE*

***Abstract*—One of the recently suggested solutions for enhancing the fuel economy and lifetime in a fuel cell (FC) hybrid electric vehicle (HEV) is the use of a multi-stack (MS) structure for the FC system. However, to fully realize the potential of this structure, the design of an appropriate energy management strategy (EMS) is necessary. This paper aims to compare the operating cost, including hydrogen consumption and degradation of the FC, between a single-stack (SS) and an MSFC-HEV. To do so, a hierarchical EMS, composed of two layers, is devised for the MS system. In the first layer, a rule-based strategy determines how many FCs should be ON according to the requested power, battery state of charge (SOC), and FCs degradations. In the second layer, an equivalent consumption minimization strategy (ECMS) is developed to determine the output power of each activated FC according to the cost function and constraints. Regarding the SS structure, ECMS is employed for power distribution. The purpose of this strategy is to decrease fuel consumption and FC system degradation costs in both structures. The performance of the ECMS is compared with dynamic programming (DP) as a global optimization strategy for validation purposes. The obtained results using experimental data show that an FC-HEV with an MS structure reaches less hydrogen and degradation costs than an SS one.**

***Index Terms*— Energy management strategy, Equivalent consumption minimization strategy, Fuel cell degradation, Fuel cell hybrid electric vehicle, Multi-stack configuration**

NOMENCLATURE

Symbols	*Definition*
P_{req}	Requested power
F_r	Rolling friction of the tires
F_{ad}	Force of aerodynamic resistance
F_a	Acceleration force
v	Vehicle velocity
M	Total mass of the vehicle
g	Gravitational acceleration
θ	Slope of the road
ρ_{air}	Air density
c_d	Aerodynamic drag coefficient
A_{ad}	Contact area of the vehicle's front surface
η_{drive}	Efficiency of the driving line
η_{em}	Efficiency of the electric motor
η_{DC-AC}	Efficiency of the DC-AC inverter
η_{DC-DC}	Efficiency of the DC-DC converter
V	FC voltage
I	FC current
H_2	FC hydrogen consumption
P_{FC}	FC power
$b_1, b_2, b_3, b_4, b_5, a_1, a_1, a_3$	Fitting coefficients
ΔV_{cell}	FC voltage degradation
$\beta_{on/off}$	FC degradation rate of start-stop cycle
β_{high}	FC degradation rate of High load
β_{low}	FC degradation rate of low load
β_{tran}	FC degradation rate of transition load
$N_{on/off}$	Number of the start-stop cycle
T_{high}	Duration of FC working under high load
T_{low}	Duration of FC working under low load
N_{tran}	Amount of load change
I_{bat}	Battery current
V_{oc}	Open-circuit voltage
SOC	Battery state of charge
R_{bat}	Battery internal resistance
P_{bat}	Battery output power
V_{bus}	Bus voltage
η_{bat}	Coulombic efficiency
Q_{bat}	Nominal battery capacity
P_{ME}	FC power at maximum efficiency
SOC_{max}	SOC maximum value
SOC_{min}	SOC minimum value
k	Time step
C_{H_2}	Total hydrogen consumption

M. Moghadari is with Hydrogen Research Institute, Electrical and Computer Engineering Department, Université du Québec à Trois-Rivières, QC, Canada (email: mohammadreza.moghadari@uqtr.ca).

M. Kandidayeni is with e-TESC and IRH labs, Department of Electrical Engineering and Computer Engineering, University of Sherbrooke, Sherbrooke, QC, J1K 2R1, Canada (email: mohsen.kandidayeni@usherbrroke.ca).

L. Boulon, is with Hydrogen Research Institute, Electrical and Computer Engineering Department, Université du Québec à Trois-Rivières, QC, Canada (email: loic.boulon@uqtr.ca).

H. Chaoui is with the Intelligent Robotic and Energy Systems (IRES) Research Group, Department of Electronics, Carleton University, Ottawa, ON, Canada (email: hicham.chaoui@carleton.ca).

$C_{H_2,FC}$	FC hydrogen consumption
$C_{H_2,bat}$	Battery equivalent consumption
α_{H_2}	Hydrogen price per kilogram
$C_{H_2,FC,avg}$	Average FC hydrogen consumption
$P_{FC,avg}$	Average FC power
η_{chg}	Battery charging efficiency
η_{dis}	Battery discharge efficiency
$\eta_{chg,avg}$	Average charging efficiency of the battery
$\eta_{dis,avg}$	Average discharge efficiency of the battery
η_{bat}	Battery efficiency
R_{dis}	Battery discharging resistance
R_{chg}	Battery charging resistance
C_{deg}	Cost of FC degradation
$C_{on/off}$	Cost of start-stop cycle degradation
C_{high}	Cost of high load degradation
C_{low}	Cost of high load degradation
C_{tran}	Cost of transition load degradation
V_{EOL}	FC end of life voltage
ζ_{stack}	Unit of FC stack price
P_{rated}	FC rated power in kW
N_{cell}	Number of cells in an FC stack
Δt	Sampling period
J_k	Total cost function
$P_{FC,max}$	FC maximum power
$P_{FC,min}$	FC minimum power
$\Delta P_{FC,max}$	FC maximum fluctuation
$\Delta P_{FC,min}$	FC minimum fluctuation
$P_{bat,max}$	Battery maximum power
$P_{bat,min}$	Battery minimum power
x_k	State variable
u_k	Control signal
t_f	Final time of the driving cycle
t_s	Sampling time

I. Introduction

Proton exchange membrane (PEM) fuel cell (FC) has been increasingly used in FC-hybrid electric vehicles (HEV) due to its high-power density, high efficiency, less noise, low operating pressure and temperature, and local-zero-emission [1]. Despite the valuable merits of an FC-HEV, some obstacles, such as hydrogen availability, the high price of components, and PEMFC reduced lifetime, have hindered its mass production compared with HEVs [2]. The US Department of Energy (DOE) has set a lifespan target of 5000 hours in a passenger vehicle for automotive PEMFCs [3]. Start-up/shutdown cycling, low-power operation, high-power operation, and fast load shifting cycles are all part of a typical automotive FC load profile. This kind of power demand on the FC stack might result in substantial reversible and permanent degradations, as well as hastened decay of the FC system [4]. As a result, it is critical to regulate the safe operation of the FC stack to a feasible extent. Using low-power FC stacks, known as a multi-stack (MS) FC system, instead of a single high-power FC stack can be considered a suitable solution to overcome some of the mentioned barriers [5], [6]. In comparison to the single-stack (SS) system, the MSFC performs well in terms of space flexibility, efficiency, and power level. In conventional FC-HEVs with one FC stack, the whole performance will change by a single FC failure. However, an MSFC can control this problem by its modularity [7], [8]. The modular design enables the failed stacks to be changed independently without affecting the overall electrical connection, hence enhancing the FC system's maintainability [9], [10]. Redundancy is one of the most important attributes of MSFC. This feature allows the whole system to continue working even in degraded mode by halting the power production of the faulty stacks. When the faulty stacks recover from unhealthy behavior, like flooding and drying out, they contribute to the overall system and begin to operate again [11]. Furthermore, the use of MSFC assists in the reduction of individual stack degradation as well as the system's overall stability [12]. The slow dynamic response is an intrinsic characteristic of an FC. To overcome this defect, using an energy storage system (ESS) like the battery alongside the FC is vital [13]. Besides, an ESS provides power peaks and regenerative energy, which helps the FC work in its efficiency range and decreases hydrogen consumption and degradation [14]. Efficient power distribution in a powertrain system with two or more power sources needs a suitable energy management strategy (EMS) as the heart of power control to ensure system drivability, fuel economy, emission reduction, and sustaining ESS state of charge (SOC) [15]. Generally, EMSs can be divided into rule-based and optimization-based approaches [16]. Optimization-based strategies are also divided into offline and online. One of the most well-known offline methods is dynamic programming (DP) which requires the driving cycle information in advance. DP is usually used as a benchmark for other optimization methods. Equivalent consumption minimization strategy (ECMS), model predictive control, and robust control are parts of online optimization strategies [17]–[19].

Due to the aforementioned benefits of the MSFC, the usage of such an architecture has been taken into consideration in different vehicular applications like passenger vehicles, heavy-duty, locomotives, and so forth, recently. On the other hand, the researchers endeavor to increase the potential, lifespan, and efficiency of the MSFC to exploit its advantages as much as possible. A hierarchical power distribution method for a dual-stack FC hybrid powertrain is suggested in [6]. This research also focuses on an online identification approach based on the forgetting factor recursive least square algorithm for updating the dual-PEMFC system's parameters in real-time. The experimental results show that the suggested strategy can improve the efficiency and performance of FC systems while lowering system fuel consumption. In [7], the authors introduce a self-adaptive EMS for an MSFC powertrain that takes into account the efficiency and health of dual-stack FC as well as overall trip costs to raise the FC's power level. The suggested EMS is projected to deal with the dynamic price fluctuations of different energy sources, lowering overall trip costs and extending the dual-stack FC's lifespan. The "equivalent fitting circle" approach is presented as the control layer method in [8]

for the system consisting of multiple FCs to tackle the energy distribution among sets of FCs with various characteristics. In comparison to other methods, the simulation results demonstrate good performance in terms of hydrogen consumption. To tackle a multi-objective power allocation strategy issue in MSFC, [9] introduces a novel decentralized convex optimization framework based on the auxiliary problem idea. To validate the benefits of the suggested method over existing centralized ones, various simulations and experimental validations are performed. In [10], a predictive soft loading approach with an enhanced overall efficiency maximization strategy is proposed for dual-stack FC systems to reduce the unfavorable loading situations that may degrade the sub-stacks. The authors of [11] suggest a bi-level optimization problem for the MSFC under constraints for stack allocation and power management. Finally, the solution findings are studied and assessed using different efficiency weights, application situations, efficiency, and Remaining Useful Life (RUL) features of accessible stacks as effect variables. In [12], an increment-oriented online power distribution strategy for MSFC is used to improve the collaboration between fuel economy and durability. In comparison to other advanced methodologies, the results show that the suggested approach can provide fault tolerance operation and collaborative performance improvement for MSFC. The authors of [20] design a power allocation method for the MSFC in order to lessen the performance gap between the FCs and prolong the system's lifespan. To execute the power distribution among four PEMFC stacks, the given approach uses the degree of performance degradation of stacks and the demand power. The results show that even if one of the stacks in the system fails unexpectedly, the MSFC can continue to function and allocate power. An online EMS for an MSFC hybrid electric vehicle is devised in [21] to improve fuel efficiency and the lifespan of the FC stacks. In this regard, a two-layer strategy for sharing power across four FCs and a battery pack is presented. The results of the proposed EMS point to a substantial increase in the system's overall performance. The study of [22] proposes a novel power distribution approach based on forgetting factor recursive least square online identification to fulfill the aim of minimizing the fuel consumption of an MSFC. The results show that the performance of the proposed power allocation strategy can be properly validated and it can provide satisfactory results.

According to the recent works on the MSFC system, one of the most significant issues in such systems is minimizing hydrogen consumption. In this respect, ECMS could be a practical choice among other online strategies since it has a viable ability to obtain optimal control quickly, which is necessary for real FC-HEVs [16], [18]. In recent years, many researchers have used ECMS to achieve the best fuel economy. In [23], ECMS is proposed for a hybrid tram where, compared to the operation mode switching method, it has saved hydrogen consumption up to 3.5%. The results indicate that the suggested EMS improves drivability and efficiency. In [24], the authors have shown that considering the maximum efficiency range in an ECMS can improve FC performance and fuel economy. In [25], an online adaptive ECMS based on power source degradation is proposed for a vehicle powered by an FC, battery, and supercapacitor. To achieve precise and reliable results of ECMS, the authors adjust the equivalent factor based on the state of health of FC and battery by using the degradation model. The authors in [26] employ SQP-based ECMS for a hybrid vehicle equipped with an FC, battery, and supercapacitor. This study shows that the proposed strategy can achieve better fuel economy compared with a rule-based control strategy.

Several advantages of MSFC systems have been documented in the literature, but the cost is still an open question. This cost could be divided between system cost and operating cost. This paper focuses on the operating cost. For this purpose, This paper puts forward a hierarchical EMS with two operating layers for an MSFC-HEV. The first layer of the strategy (rule-based) decides on the number of FCs that should be ON, and the second layer (optimization-based) is accountable for distributing the power among the active FCs and the battery pack by means of ECMS. The operating cost of the MS system, including hydrogen (FC and battery equivalent consumption), and FC degradation, is compared with an SS one. In this regard, DP is used as a benchmark to confirm the obtained results based on ECMS. From the conducted literature study, the novelties of this paper are:

1- Comparing the total operating cost (hydrogen and degradation costs) between an SS and an MSFC-HEV: prior research on MSFC lacks an analytical comparison of the operational costs between the two systems.
2- Designating the number of active FCs in the MS system by devising a hierarchical EMS: To achieve the lowest operational cost, this research proposes a hierarchical energy management strategy. Controlling hydrogen consumption and FC degradation in an MSFC system is largely reliant on how each FC operates. It is critical that FCs operate in a different way in order to reduce system operating costs. A rule-based layer is developed to decide how many FCs should participate in the multi-objective cost function at each time step depending on the requested power, battery SOC, and health state of each FC.
3- Taking into account FC degradation terms alongside hydrogen consumption for an MS configuration: The majority of ECMS articles concentrate on reducing hydrogen consumption without taking into account the cost of FC degradation.

The rest of this paper is organized as follows. Section II describes the vehicle modeling. EMS explanation is provided in section III. Section IV discusses the achieved results, and the conclusion is given in section V.

II. MODELING

A. Vehicle structure and powertrain configuration

This paper investigates a hybrid powertrain with two different configurations: one is an SSFC, and another is an MSFC system. Fig. 1 displays the MS powertrain that utilizes four 500-W PEMFCs, as the primary power sources, with a battery pack. For the SS system, a 2000-W FC substitutes the four 500-W PEMFCs. Both configurations follow a semi-active principle where FCs are connected to the DC bus through unidirectional DC-DC converters while the battery pack is linked to the bus directly without any converters [21], [24]–[26]. The requested power from the driving cycle (P_{req}) can be calculated by (1) based on longitudinal dynamics of a road vehicle:

$$P_{req} = v\,F_{req} = (F_r + F_{ad} + F_a)\,v \quad (1)$$

$$\begin{cases} F_r = c_r\, M\, g\, \cos(\theta) \\ F_{ad} = \dfrac{1}{2}\rho_{air}\, c_d\, A_{ad}\, v^2 \\ F_a = M\dfrac{dv(t)}{dt} \end{cases} \quad (2)$$

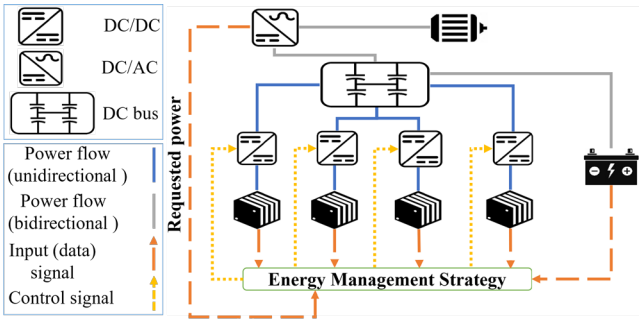

Fig. 1. Powertrain structure for the MS system.

Where F_r is the rolling friction of the tires, F_{ad} is the force of aerodynamic resistance, F_a is the acceleration force, v is the vehicle speed. The FC-HEV that is employed in this paper is Nemo. Table. I shows the vehicle's specifications [27].

The battery and the FC supply the requested power imposed by the driving cycle, and their power merge in the DC bus (P_{dc}) is given by (3).

$$P_{dc} = P_{bat} + P_{FC}\,\eta_{DC-DC} = \begin{cases} \dfrac{P_{req}}{\eta_{drive}\,\eta_{em}\,\eta_{DC-AC}}, & P_{req} \geq 0 \\ P_{req}\,.\,(\eta_{drive}\,\eta_{em}\,\eta_{DC-AC}), & P_{req} < 0 \end{cases} \quad (3)$$

Where η_{drive}, η_{em}, η_{DC-AC} and, η_{DC-DC} are the efficiency of the driving line, electric motor, DC-AC inverter, and DC-DC converter, respectively.

B. Fuel cell model

As mentioned before, PEMFC is used as the primary power source. In this paper, two PEMFCs with different power rates but produced with the same technology are employed. As one of the goals of this study is to compare the operating cost of an SSFC-HEV with an MS one, it is vital to utilize the FCs with the same technology to avoid any confusion in the comprehension of the obtained results. The first FC is the Horizon 2000-W used in the SS configuration, and the second one is the Horizon 500-W employed in the MS structure. These FC technologies have been used in other studies as well [9], [21], [28], [29].

TABLE I
VEHICLE SPECIFICATIONS

Parameters	Value
Coefficient of rolling friction c_r	0.015
The total mass of the vehicle M	896 kg
Gravitational acceleration g	9.81 m/s^2
The slope of the road θ	0°
Air density ρ_{air}	1.2 kg/m^3
Aerodynamic drag coefficient c_d	0.42
The contact area of the vehicle's front surface A_{ad}	4 m^2
Top speed	40 km/h

The curves of Horizon 2000-W and Horizon 500-W have been obtained from a developed test bench presented in Fig. 2. Both FCs are open cathode and air-cooled.

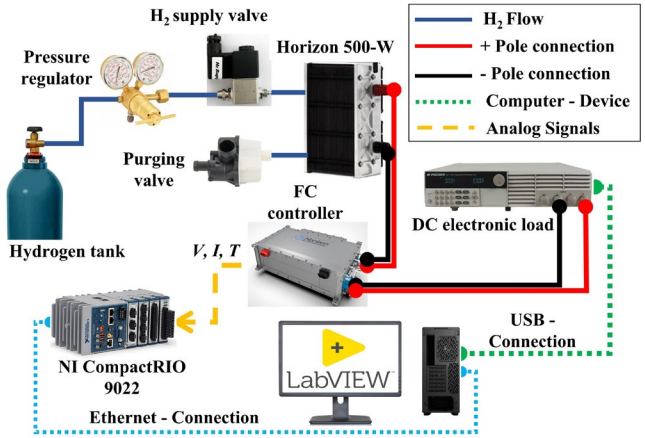

Fig. 2. The PEMFC test bench in the Hydrogen Research Institute of Université du Québec à Trois-Rivières (UQTR).

Due to the low-power nature of the application, the open cathode FC (air-cooled) is employed in this study. The vehicle under investigation is a low-speed vehicle with a maximum speed of 40 km/h. Open cathode FCs are suggested for this range of power applications [30].The main components of each FC include an FC stack and some auxiliaries, such as a cooling fan and hydrogen supply subsystem. Therefore, the net produced power of the FC system is equal to the difference between produced power from the stack (P_{stack}) and the used power from the auxiliary components (P_{aux}). The specification of each FC system is listed in Table. II. The presented set-up in Fig. 2 has been developed in Hydrogen Research Institute of Université du Québec à Trois-Rivières (UQTR). This figure shows that a Horizon 500-W is connected to a National Instrument CompactRIO using the PEMFC controller. For an SS system, the Horizon 2000-W is substituted for 500-W in the test bench. The pressure of hydrogen is set between 0.5 and 0.6 bar. The hydrogen supply valve, located on the anode side, provides dry hydrogen for the PEMFC stack, and its flow rate is between 0 and 7 $\frac{l}{min}$ according to the drawn power from the stack. On the anode outlet, the purge valve is responsible for removing excess hydrogen, water, and nitrogen every 10 s with a duration of 100 ms. An Ethernet connection transfers the data between the CompactRIO and the PC every 100 ms, then FC system voltage, current, and temperature are recorded. For requesting load profiles from the PEMFC, an 8514 BK Precision DC Electronic Load is utilized.

TABLE II
FUEL CELLS SPECIFICATION

FC technology / Characteristics	Horizon 2000-W (PEM)	Horizon 500-W (PEM)
Number of cells	48	24
Rated Power	2000 W	500 W
Voltage range	24-43 V	12-23 V
Maximum current	78 A	40 A
Weight (with fan & casing)	10 kg (±200grams)	2.52 kg (±50grams)

Fig. 3 shows the polarization, hydrogen consumption, and FC system efficiency curves of the Horizon 2000-W PEMFC, where the solid black lines are the experimental reference curves, and the red dashed lines illustrate the fitted models. Fig. 4 displays the polarization, hydrogen consumption, and FC

system efficiency curves of Horizon 500-W.

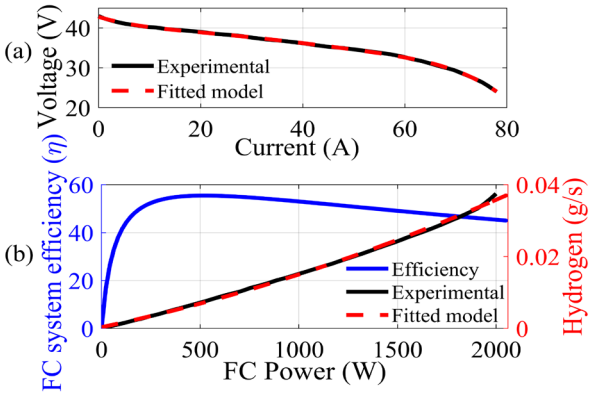

Fig. 3. The characteristic curves of the Horizon 2000-W: (a) polarization curve; (b) hydrogen consumption and efficiency curve.

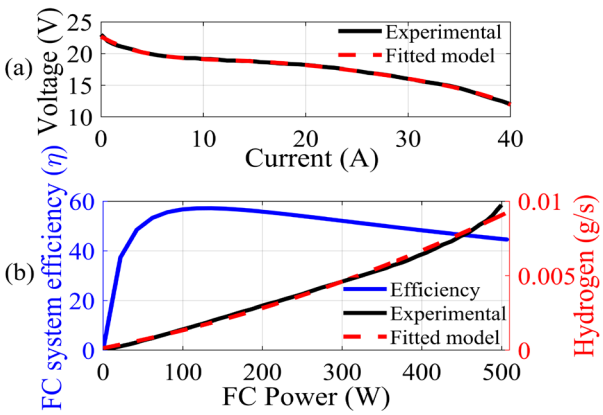

Fig. 4. The characteristic curves of the Horizon 500-W: (a) polarization curve; (b) hydrogen consumption and efficiency curve.

The fitted polarization and hydrogen consumption models are a polynomial function of current and FC power, as shown in (4)-(5).

$$V(I) = b_1 I^4 + b_2 I^3 + b_3 I^2 + b_4 I + b_5 \quad (4)$$

$$H_2(P_{FC}) = a_1 P_{FC}^2 + a_2 P_{FC} + a_3 \quad (5)$$

The values of all the coefficients in (4)-(5) for Horizon 2000-W and Horizon 500-W are introduced in Table. III.

TABLE III
COEFFICIENT VALUES OF (4)-(5)

Equation (4)		
Coefficients (unit)	Values	
$b_1(\frac{V}{A^4})$, $b_2(\frac{V}{A^3})$, $b_3(\frac{V}{A^2})$, $b_4(\frac{V}{A})$, $b_5(V)$	FC 2000-W	FC 500-W
	-7.8×10^{-7}, 4.934×10^{-5}, 5.832×10^{-4}, -0.207, 42.41	1.353×10^{-5}, -0.001, 0.046, -0.663, 22.390
Equation (5)		
Coefficients (unit)	Values	
$a_1(\frac{g}{W^2})$, $a_1(\frac{g}{W})$, $a_3(g)$	FC 2000-W	FC 500-W
	3.050×10^{-9}, 1.190×10^{-5}, 8.253×10^{-4}	1.470×10^{-8}, 1.080×10^{-5}, 2.450×10^{-4}

FC degradation is a natural and inevitable phenomenon that can lead to voltage decrease and performance loss. Choosing and designing a suitable EMS has a crucial role in slowing down the FC degradation and increasing its lifetime by avoiding the operation in high and low power for an extended period and decreasing high and frequent transition loads [31]. Each component of a PEMFC has its degradation mechanism, so focusing on the degradation of the component level and its relation and effects on the other components cannot be covered and are hard to reach. Therefore, the FC degradation modeling is normally considered at the stack level [32]. The rate of degradation will change based on the FC technology used, as well as the operating conditions. In fact, developing a comprehensive degradation model for an FC system is still an area of investigation [32], [33].

According to the above descriptions, four operating conditions of PEMFC are known as primary degradation factors. These four operating conditions are start-stop cycle, high load, low load, and transition load [32], [34], [35]. The start-stop cycle, which is the FC on/off, has a predominant and adverse effect on voltage degradation, and it can decrease FC voltage enormously [34], [36]. For other factors of degradation, high loading is described as when $P_{FC} \geq 0.8\, P_{FC,max}$ and low loading is defined as when $P_{FC} \leq 0.2\, P_{FC,max}$. In Horizon 500-W and 2000-W, $P_{FC,max}$ are 500 W and 2000 W, respectively. The transition load is considered as the absolute value changes of the FC output power [34]–[36]. Equation (6) illustrates the total voltage degradation (μV) of a cell [34]–[36]:

$$\Delta V_{cell} = \beta_{on/off}\, N_{on/off} + \beta_{high}\, \frac{T_{high}}{3600} + \beta_{low}\, \frac{T_{low}}{3600} + \beta_{tran}\, N_{tran} \quad (6)$$

Where β_{high}, β_{low}, $\beta_{on/off}$, and β_{tran} are the degradation of voltage cell rate per hour ($\frac{\mu V}{h}$), per cycle ($\frac{\mu V}{cycle}$), and per kilowatt ($\frac{\mu V}{kW}$) for each high load, low load, start-stop cycle, and transition load, respectively. The degradation rates are listed in Table. IV. $N_{on/off}$ denotes the number of the start-stop cycle during a driving cycle, T_{high}, and T_{low} are the duration that FC works under high and low load (in second), and $N_{tran} = |\Delta P_{FC}| = P_{FC}(t) - P_{FC}(t-1)$ is the amount of load change. It is worth noting that $|\Delta P_{FC}|$ refers to the absolute change in FC power between two consequent points. To clarify, $|\Delta P_{FC}|$ is defined as the difference in the FC power of time steps *t* and *t-1* during the driving cycle. In each time step in the simulation, ΔV_{cell} is deducted from the FC voltage. The accuracy of the degradation model is not the main focus of this study. The major emphasis is on the strategy's performance when the FCs degrade. The employed degradation model to evaluate the strategy's performance has been used in a number of papers [9], [34], [35], [37].

TABLE IV
THE RATE OF PEMFC DEGRADATION (CELL LEVEL)

Operating condition	Degradation rate	Data reference
Start-stop cycle ($\beta_{on/off}$)	13.79 $\frac{\mu V}{cycle}$	[34], [35], [37]
High load (β_{high})	10.00 $\frac{\mu V}{h}$	[34], [35], [37]
Low load (β_{low})	8.66 $\frac{\mu V}{h}$	[34], [35], [37]
Transition load (β_{tran})	0.0441 $\frac{\mu V}{kW}$	[34], [35], [37]

C. Battery model

As mentioned earlier, an ESS in an FC-HEV is necessary to assist FC with operating in its efficient zone and decrease the degradation by absorbing peak powers and supplying low

powers of the driving cycle [36]. Therefore, in this paper, a lithium-ion battery is employed as an ESS. For modeling the battery, this paper uses the internal resistance-based model [29]. Fig. 5 illustrates the equivalent circuit of the battery model. The features of the battery are listed in Table. V.

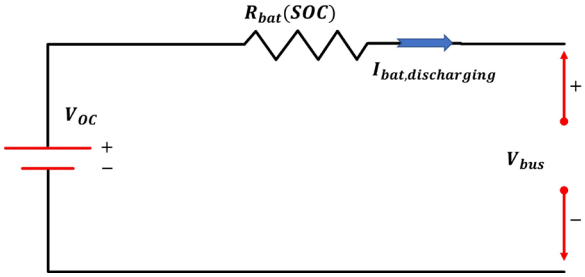

Fig. 5. Equivalent circuit of the battery model [29].

TABLE V
SPECIFICATION OF THE BATTERY

SAFT Rechargeable lithium-ion battery cell	
Capacity	6 Ah
Maximum current continuous	C/1 A
Nominal voltage	3.65 V
Number of cells in series	20
Coulombic efficiency	0.99
Cell mass	0.34 kg

It is important to note that the battery current (I_{bat}) flows in a positive direction while the battery is discharging and in a negative direction when it is charged. The relation of open-circuit voltage and internal resistance with battery SOC is presented in Fig. 6. The utilized battery data have been extracted from experimental tests performed by the National Renewable Energy Laboratory [29]. Equations (7), (8), and (9) show the battery current (I_{bat}), bus voltage (V_{bus}), and SOC.

$$I_{bat} = \frac{V_{oc} - \sqrt{V_{oc}^2(SOC) - 4\,R_{bat}(SOC)\,P_{bat}}}{2\,R_{bat}(SOC)} \tag{7}$$

$$V_{bus} = V_{oc}(SOC) - I_{bat}\,R_{bat} \tag{8}$$

$$SOC(t) = SOC(t_0) - \eta_{bat}\,\frac{\int_{t_0}^{t} I_{bat}\,dt}{Q_{bat}} \tag{9}$$

Where $P_{bat} = I_{bat}\,V_{bus}$, V_{oc} and R_{bat} are the open-circuit voltage and battery internal resistance and can be expressed as a function of SOC. P_{bat} is the battery output power, Q_{bat} is the nominal battery capacity (Ah), and η_{bat} is the Coulombic efficiency.

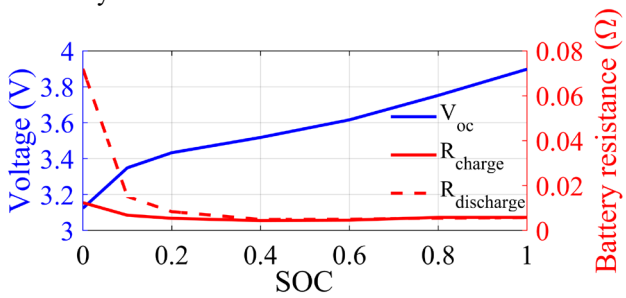

Fig. 6. The correlation of SOC with battery open-circuit voltage and resistance.

III. ENERGY MANAGEMENT STRATEGY

The primary purpose of this paper is to compare operating costs, including hydrogen cost, FC degradation cost, and total cost between the SS (Horizon 2000-W) and the MSFC system (four Horizon 500-W). In this regard, a hierarchical EMS, as shown in Fig. 7, is developed for the MS system. In the first layer, a rule-based strategy is used to determine how many FCs should be ON according to the requested power, SOC, and FCs degradation rate. The second layer employs ECMS to determine the output power of each FC to satisfy the requested power while minimizing the defined cost function. ECMS as an optimization-based EMS is used for two principal purposes: reducing the total hydrogen consumption (FC and battery equivalent consumption) and FC degradation. Regarding the battery pack, the necessary constraints are considered to enhance its lifetime. Obviously, such problems are known as multi-objective problems, and there is always a trade-off between different purposes. Since ECMS is a local optimization strategy, this paper uses DP as a global optimization strategy to validate the achieved results. Regarding the SS configuration, ECMS is utilized to distribute the power between the FC and the battery pack.

A. First layer: Rule-based

In the first layer of this hierarchical EMS, a rule-based strategy determines the number of FCs that should participate in the optimization problem based on the requested power, SOC, and FCs degradation rate. The primary purpose of this strategy is to activate the minimum number of FCs to meet the requested power considering the age and other constraints. In each step, the voltage drop from previous times is collected until the current time step and then subtracted from the FC voltage (equation (4)). The output power of the FC is lowered by decreasing the voltage in each step according to the circumstances in which each FC operates. As a result, the FC or FCs with the lowest voltage drop or greatest maximum power are regarded the youngest FCs and have the highest priority to participate in the optimization algorithm at each time step. For instance, if two FCs are adequate to provide the requested power, the two least degraded FCs will be ON, and the other two that are most degraded operate at their maximum efficiency point (P_{ME}). FC ON means that it can operate between minimum power and maximum power in its whole domain. This strategy aims to prevent the most degraded FCs from more degradation. The most degraded FCs will not be OFF because start-stop cycles increase the degradation dramatically. The reason for working at the maximum efficiency point is that at this point, the hydrogen consumption is minimal, and the degradation rate is mild as it is between high load and low load limitation.

Table. VI shows the rules of this strategy. The maximum and minimum values of SOC are 90% and 50%, respectively.

B. Second layer: Equivalent consumption minimization strategy

In the second layer, ECMS is utilized as an optimization algorithm to designate the output power of each FC activated in the first layer.

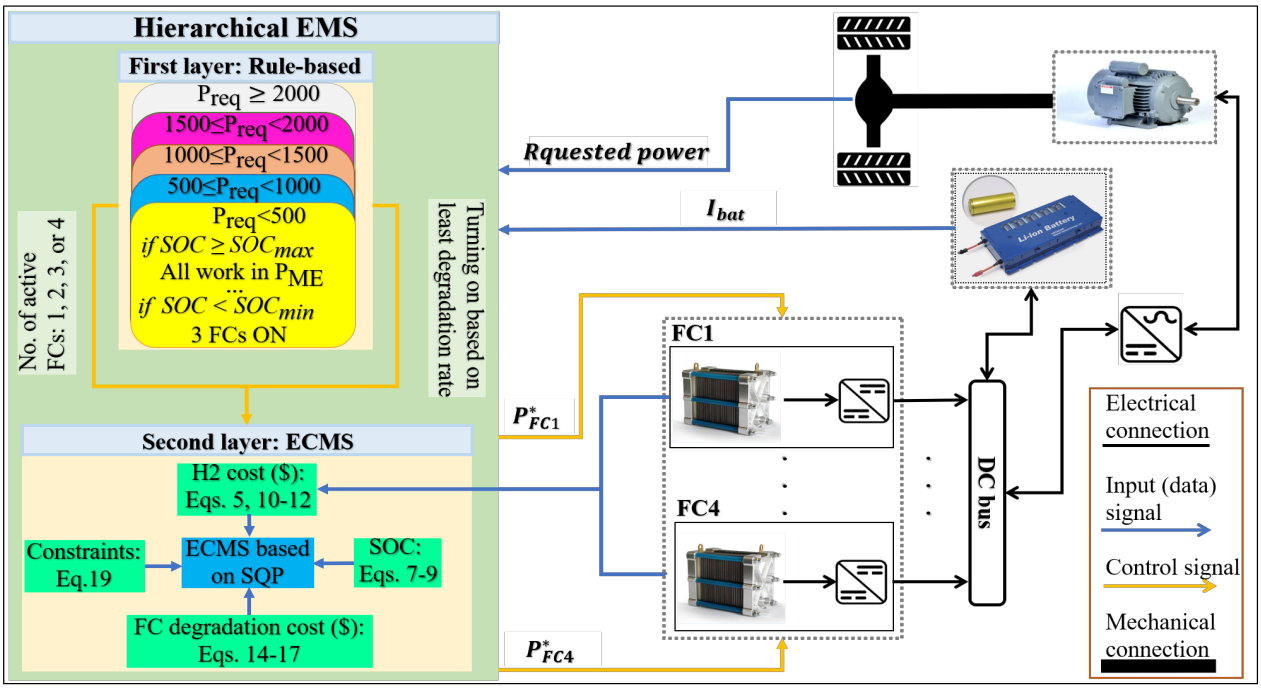

Fig. 7. The concept of the proposed hierarchical EMS.

TABLE VI
RULE-BASED STRATEGY

Conditions \ P_{req}	Range of P_{req} (kW)				
	<0.5	0.5−1	1−1.5	1.5−2	>2
	Number of active FCs				
SOC≥SOC$_{max}$	All P$_{ME}$	All P$_{ME}$	1 FC	2 FCs	3 FCs
80%≤SOC<SOC$_{max}$	All P$_{ME}$	All P$_{ME}$	1 FC	2 FCs	3 FCs
70%≤SOC<80%	1 FC	1 FC	2 FCs	3 FCs	3 FCs
60%≤SOC<70%	2 FCs	2 FCs	3 FCs	3 FCs	4 FCs
SOC$_{min}$≤SOC<60%	2 FCs	3 FCs	4 FCs	4 FCs	4 FCs
SOC<SOC$_{min}$	3 FCs	4 FCs	4 FCs	4 FCs	4 FCs

The output power of each FC is determined so that the minimum value of the cost function is obtained. The concept of ECMS is to convert electrical energy from ESS to the equivalent hydrogen consumption to minimize the total hydrogen consumption of the system [23]–[26], [38]. In this paper, alongside the cost of hydrogen consumption, FC degradation is added to the cost function. Indeed, in this problem, the optimization algorithm chooses its optimal control decision by minimizing the total cost of the cost function. Therefore, the cost function is introduced in two parts: the definition of hydrogen consumption cost and FC degradation. SQP algorithm is one of the powerful methods to solve constrained nonlinear optimization problems. SQP uses a series of quadratic programming sub-problems to reach a minimum value of a cost function [24]–[26], [34], [39]. Indeed, in this paper, SQP solves the ECMS by finding a suitable FC power as a control variable to minimize the cost function. The SQP is programmed in MATLAB to solve the ECMS problem in real-time.

I. Multi-objective cost function

According to the concept of ECMS, the total hydrogen consumption is the sum of the hydrogen consumption on the FC side and the equivalent hydrogen consumption on the battery side. Equation (10) describes the hydrogen consumption cost in the multi-objective cost function. The required units for the following equations are introduced in the parentheses.

$$C_{H_2,k} = (C_{H_2,FC,k} + C_{H_2,bat,k})\,\alpha_{H_2}\ (\$) \tag{10}$$

Where $C_{H_2,FC,k}$ is the FC hydrogen consumption over the time step k that is a polynomial function of FC output power according to (5). The battery equivalent consumption is a function of FC average hydrogen consumption, FC average power, battery power, and battery charge and discharge efficiencies as explained in (11). α_{H_2} is the hydrogen price per kilogram, so the hydrogen consumption must be in kg.

$$C_{H_2,bat,k} = \begin{cases} \dfrac{P_{bat,k}}{\eta_{chg,avg}\,\eta_{dis}}\,\dfrac{C_{H_2,FC,avg}}{P_{FC,avg}}\ (g), & P_{bat} \geq 0 \\ P_{bat,k}\,\eta_{dis,avg}\,\eta_{chg}\,\dfrac{C_{H_2,FC,avg}}{P_{FC,avg}}\ (g), & P_{bat} < 0 \end{cases} \tag{11}$$

In the above equation, $C_{H_2,FC,avg}$ is the average FC hydrogen consumption, $P_{FC,avg}$ is the average FC power, $P_{bat,k}$ is the battery power over the time step k. η_{dis} is the battery discharge efficiency, $\eta_{chg,avg}$ is the average charging efficiency of the battery, η_{chg} is the charging efficiency of the battery, and $\eta_{dis,avg}$ is the battery average discharge efficiency. The battery charge and discharge efficiencies are derived from (12):

$$\eta_{bat} = \begin{cases} \dfrac{1}{2}\left(1 + \sqrt{1 - \dfrac{4\,R_{dis}\,P_{bat}}{V_{oc}^2}}\right), & P_{bat} \geq 0 \\ \dfrac{2}{\left(1 + \sqrt{1 - \dfrac{4\,R_{chg}\,P_{bat}}{V_{oc}^2}}\right)}, & P_{bat} < 0 \end{cases} \tag{12}$$

Where R_{dis} is the battery discharging resistance, and R_{chg} is the battery charging resistance, and V_{oc} is the battery open-circuit voltage. According to (11)-(12), in discharge mode, η_{dis} and the battery recharge efficiency by the FC system ($\eta_{chg,avg}$) are taken into consideration for calculating the battery power. However, in the charging mode, P_{bat} is weighted by η_{chg} and whether the battery has previously been discharged ($\eta_{dis,avg}$). Aside from the cost of hydrogen consumption, this paper considers the degradation cost consisting of start-stop, high load, low load, and transition load. Equation (13) shows the degradation cost.

$$C_{deg,k} = C_{on/off,k} + C_{high,k} + C_{low,k} + C_{tran,k} \tag{13}$$

Where $C_{on/off}$ is the cost of start-stop cycle degradation that can be calculated as the following equation:

$$C_{on/off,k} = \frac{\beta_{on/off}\, N_{on/off,k}}{V_{EOL}}\, \zeta_{stack}\, P_{rated}\ (\$) \tag{14}$$

Where $N_{on/off,k}$ is the number of start-stop cycles over the time step of k, V_{EOL} is the voltage drop until a single PEMFC end of life which is a 10% decrease in the FC voltage. A cell approaches the end of its life when the cell voltage of an FC decreases to 10% of its nominal voltage, according to the literature study [34], [35], [37]. ζ_{stack} is the unit of FC stack price, and P_{rated} is FC rated power (in kW). The degradation cost caused by the high and low load can be described in (15) and (16):

$$C_{high,k} = \frac{\beta_{high}\, \frac{T_{high,k}}{3600}}{V_{EOL}}\, \zeta_{stack}\, P_{rated}\ (\$) \tag{15}$$

$$C_{low,k} = \frac{\beta_{low}\, \frac{T_{low,k}}{3600}}{V_{EOL}}\, \zeta_{stack}\, P_{rated}\ (\$) \tag{16}$$

Where $T_{high,k}$, and $T_{low,k}$ are the duration of the high and low load over the time step of k. The index k determines each time step, which lasts one second. To reduce FC degradation and overall operating cost, the optimization method seeks to prevent FCs from working at their high and low loads at each time step. The values of $T_{high,k}$, and $T_{low,k}$ will be 1 if FC operates in its high or low load, in time step k, since the FC works for one second in these loads. The last part of the degradation cost is related to the transition load cost shown in (17).

$$C_{tran,k} = \frac{\beta_{tran}\, (|P_{FC}(k) - P_{FC}(k-1)|)\, \Delta t}{V_{EOL}\, N_{cell}}\, \zeta_{stack}\, P_{rated}\ (\$) \tag{17}$$

Where N_{cell} is the number of cells in a stack, and Δt is the sampling period which equals 1 second.

Finally, the total cost function can be written as (18):

$$\begin{aligned} J_k = C_{H_2,k} + C_{deg,k} &= (C_{H_2,FC,k} + C_{H_2,bat,k})\, \alpha_{H_2} \\ &+ C_{on/off,k} + C_{high,k} + C_{low,k} + C_{tran,k} \end{aligned} \tag{18}$$

Regarding the cost function of the MS, each stack has a degradation cost and a hydrogen cost; therefore, the final operating cost will be the sum of the four FC stacks. The values of hydrogen consumption and unit of FC stack price are provided in Table. VII.

TABLE VII
OPERATING COST PARAMETERS

Parameter	Value	Unit	Data reference
PEMFC stack price (ζ_{stack})	93.00	\$/kW	[34], [35]
P_{rated}	2 and 0.5	kW	[34], [35]
Hydrogen price (α_{H_2})	4.00	\$/kg	[34], [35]
V_{EOL}	60000	μV	[34], [35]

II. Constraints

In an optimization problem, various constraints are vital to ensure that the powertrain components work in normal conditions and the optimal control decision is acceptable. Reactant flows, heat management, and water content in the streams and inside the FC all influence the PEMFC dynamic reaction, and they need to be controlled for the optimum operation of FCs when the system experiences varying load changes [40]. Generally, a dynamic load fluctuation cycle is defined by a sudden change from low current to maximum current in degradation tests [37]. However, in the energy management design, a conservative transition is usually considered. In this work, a dynamic limitation of 50 W/s and 200 W/s, which implies 10% of the maximum power per second is considered for the operation of the FCs [41]–[43]. For these reasons, several constraints must be applied to the FC and battery. Equation (19) shows these constraints.

$$\begin{cases} P_{FC,min} \le P_{FC,k} \le P_{FC,max} \\ \Delta P_{FC,min} \le P_{FC}(k) - P_{FC}(k-1) \le \Delta P_{FC,max} \\ SOC_{min} \le SOC(k) \le SOC_{max} \\ P_{bat,min} \le P_{bat,k} \le P_{bat,max} \end{cases} \tag{19}$$

All the parameters in the mentioned constraints are shown in Table. VIII.

C. Dynamic programming (DP)

As explained in the previous parts, DP is one of the most well-known benchmarks in optimization problems. The essence of DP is that it is aware of what happens in the future to choose the best optimal control decision. One of the weaknesses of DP is that it cannot be used in real-time problems because it needs complete driving cycle information in advance and is highly time-consuming. DP is a good choice for solving a wide range of optimization problems like nonlinear, constrained, time-variant, and discrete-time [44]. According to the pros and cons of DP, this method is a suitable criterion to validate the results of local optimization methods like ECMS. This paper utilizes the MATLAB function introduced in [44] to solve this problem with the DP algorithm. In the DP, the first step is to determine the state and control variables. In this paper, SOC is considered as the state variable (x_k) and FC power is considered as the control signal (u_k). The next step is to discretize the continuous-time model to the discrete-time model, as shown in (20).

TABLE VIII
VALUES OF CONSTRAINT PARAMETERS

Parameter	Value		Unit
	FC 2000-W	FC 500-W	
$P_{FC,min}$, $P_{FC,max}$	0, 2000	0, 500	Watt
$\Delta P_{FC,min}$, $\Delta P_{FC,max}$	-200, 200	-50, 50	Watt
SOC_{int}, SOC_{min}, SOC_{max}	70%, 50%, 90%		%
$P_{bat,min}$, $P_{bat,max}$	-1000, 1000		Watt

$$\begin{cases} x_{k+1} = F(x_k, u_k) + x_k, \quad k = 0,1,\dots,N-1 \\ x_k = SOC \\ u_k = P_{FC} \\ N = \dfrac{t_f}{t_s} + 1 \end{cases} \tag{20}$$

Where t_f is the final time of the driving cycle and t_s is the sampling time. For the MS problem, DP has four control signals as four FCs exist in this configuration. A cost function like ECMS aims to minimize operating costs by reducing hydrogen consumption and degradation costs. Concerning the constraints, the same ones defined for ECMS are used in the DP problem. According to the following objective function, by the trade-off between hydrogen consumption and FC degradation, the best values of FC power as the control variable are chosen to minimize the total operating cost.

$$J = min \sum_{k=0}^{N-1} \left(C_{H_2}(P_{FC,k}, k) + C_{deg}(P_{FC,k}, k) \right) \tag{21}$$

IV. Result and Discussion

In this section, the SS and the MS system results are compared to illustrate which one has a lower operating cost and is more reasonable to be used in a real FC-HEV. For this purpose, two different driving cycles, WLTC-class3 and FTP-75, are employed to test the performance of each case study in terms of hydrogen consumption, degradation, and total costs. The results of the two FC configurations under each driving cycle are compared with DP to illustrate the validation of the proposed EMS. The utilized driving cycles are shown in Fig. 8, where the right vertical axis shows the power (W), and the left one shows the velocity (m/s).

A. Obtained results under WLTC-class3 driving cycle

Fig. 9 shows the comparison of FC power distribution between the SS and the MS for the WLTC-class3. Fig. 9(a-d) and Fig. 9(e) illustrate the FC power distribution of the MS and SS structures using DP and ECMS, where colored lines and black lines display the power distribution for ECMS and DP, respectively. As shown in Fig. 9(a-d), to lower the overall cost of the system, the optimization algorithm prefers to utilize the battery over FCs in the period 0–1550s. Due to the high cost of an ON/OFF cycle, the optimization algorithm prefers not to switch off FCs. Each ON/OFF cycle greatly raises the system's cost.

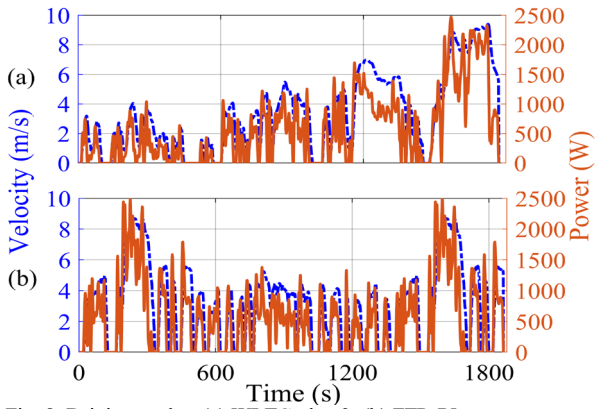

Fig. 8. Driving cycles: (a) WLTC-class3; (b) FTP-75.

As a result, the ECMS algorithm selects the ideal operating point to decrease hydrogen consumption and FC degradation while lowering overall cost. The ECMS approach prefers that each FC operates at its maximum efficiency point between 0 and 1550 seconds since, during this period, each FC not only avoids the ON/OFF cycle but also has the best fuel economy.

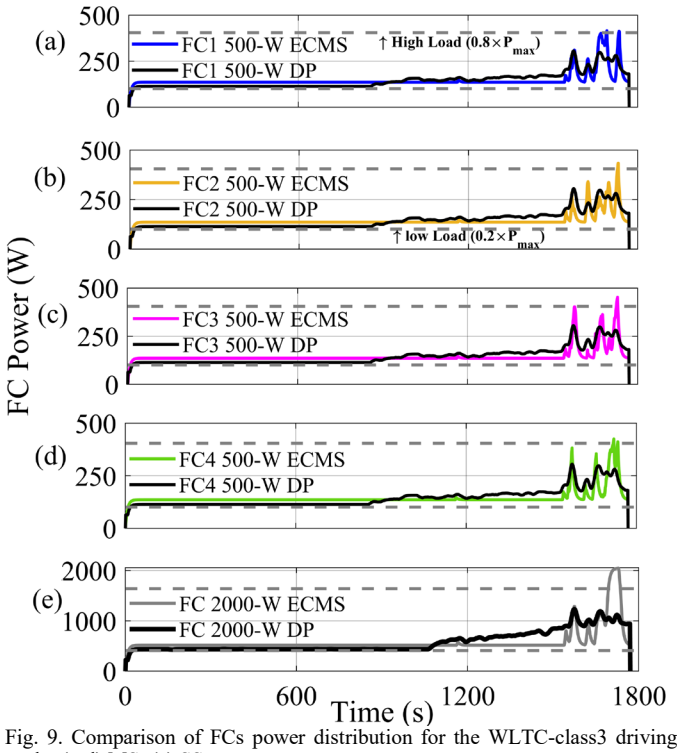

Fig. 9. Comparison of FCs power distribution for the WLTC-class3 driving cycle: (a-d) MS; (e) SS.

DP shows the same tendency in the FC power distribution. The driving cycle has high velocities within 1551–1800s time range. Therefore, FCs should work at a higher power level during this time since the requested power has increased. Indeed, it is at this time that FCs begin to operate differently. Working differently allows each FC to consume less hydrogen and degrade less than the SS system.

The mentioned explanations are true for the SS system. As shown in Fig. 9(e), the SS system works more time in the high load zone because it does not have the modularity and flexibility of the MS system. According to the feature of DP that is aware of what happens in the future in advance, it reduces FC degradation cost more than ECMS, and FCs work less in the high load zone in the DP algorithm in comparison with ECMS. Fig. 10 describes the battery SOC regarding the SS and the MS configurations using ECMS and DP algorithms. Although the EMS chooses to make the battery work harder than FC in the 0–1550s, SOC rises in certain time intervals since the driving cycle consists of low and medium velocities and the requested power is not high. Because the driving cycle throughout the 1551–1800s includes high velocities and high requested power, the battery should work harder alongside the FCs. As a result, the SOC drops more during this period. The most significant aspect is that the SOC in the MS system, SS system, and DP algorithm should all end at the same point in order to compare them fairly. To guarantee that all these algorithms achieve the same final SOC, the final SOC related to SS is imposed on the SOC of MS and the DP algorithm as a terminal SOC. Since DP tries to reach

a minimum cost at the end of the cycle while ECMS minimizes the cost function at each time step, the SOC trend between DP and ECMS is different.

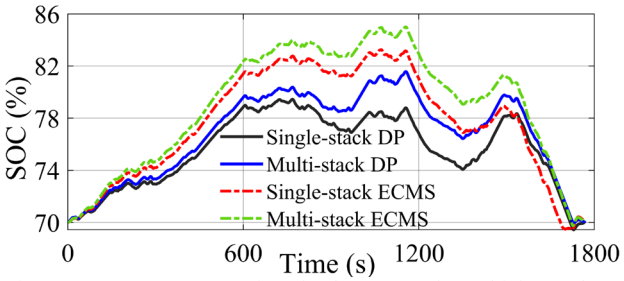

Fig. 10. Battery SOC comparison for the WLTC-class3 driving cycle.

Fig. 11 represents the operation of the SS and MS systems in the safe zone. The safe zone is an area between the power of maximum efficiency and high load ($0.8\ P_{max}$) zones [21]. This figure can illustrate clearly why an MS system is more efficient than an SS system. As is seen, in the MS system (Fig. 11(a)), 99.4% of the FCs power is in the safe zone in the total time of the driving cycle, while in the SS system (Fig. 11(b)), this amount decreases to 97%. In fact, the MS system works 2.4% more than the SS system in the safe zone. This difference in operation leads to fewer operating cost for the MS system.

According to Fig. 12, each FC in the MS system has a slower degradation rate than the utilized FC in the SS system. DP, as a benchmark, has fewer voltage drops for both 2000-W and 500-W FCs. When one FC degrades more than other FCs, the system uses the most degraded one less than others to avoid further degradation, thanks to the modularity and flexibility of the MS system. If an FC operates in a high load zone for a long time in the MS system, however, the system can reduce the power of the most degraded FC while boosting the usage of the other FCs. Because there is no other option or flexibility in an SS system, the high-power FC must continue to operate in the high load zone. Therefore, it is evident that an FC in the SS system has a faster degradation than that of the MS system. From Fig. 12(b), in the SS system, the difference in degradation of DP and ECMS is more significant than the MS system. This stems from the fact that the FC in an SS system spends more time in the high load zone than the FCs in an MS system, as shown in Fig. 9(e). Working in the high load zone intensifies the FC's degradation and reduces its lifetime. As is seen in Fig. 9(e), ECMS, which is a real-time strategy, keeps working at maximum efficiency point until 1550 s. Then, the FC power experiences a striking increase and keeps working at the high load zone. However, in the case of DP which is aware of the whole driving cycle in advance, the FC operates at the maximum efficiency point for 1000s. After that, the FC power gradually increases to meet the requested power, and therefore it works in the high load zone less than the ECMS.

Fig. 13 shows the hydrogen consumption of the SS and MS systems. The results confirm that the MS configuration consumes less hydrogen than the SS system. According to the obtained results by DP and ECMS, the hydrogen consumption of the MS system is 3.173% and 3.852% less than the SS one, respectively. This lower hydrogen consumption is also in agreement with the presented results in Fig. 11, based on which the MS system works in the safe zone more than the SS.

B. FTP-75 driving cycle

Fig. 14 describes the battery SOC regarding the SS and the MS configurations using ECMS and DP algorithms. It should be said again that the most important thing about comparing MS systems, SS systems, and DP algorithms is that they all must finish in the same SOC.

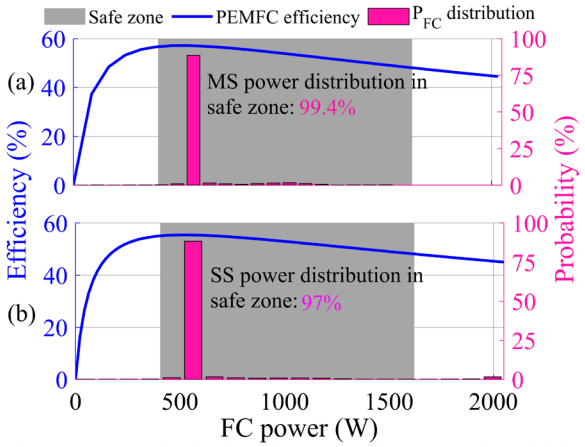

Fig. 11. FC operating in the safe zone for the WLTC-class3 driving cycle: (a) MS; (b) SS.

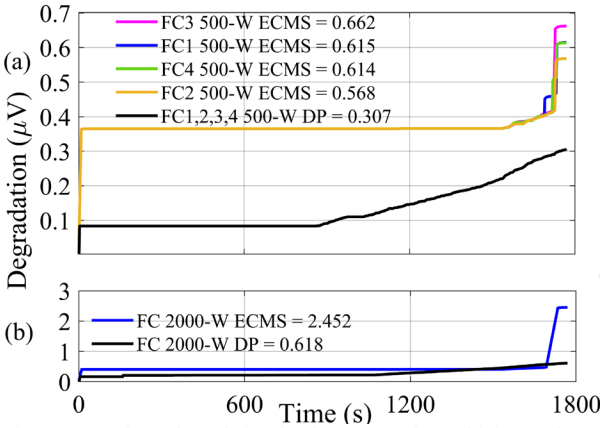

Fig. 12. FC voltage degradation for the WLTC-class3 driving cycle: (a) MS; (b) SS.

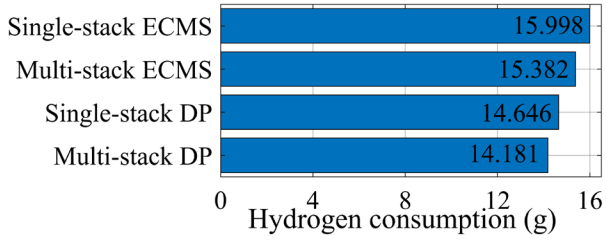

Fig. 13. Hydrogen consumption comparison between the MS and the SS for the WLTC-class3 driving cycle.

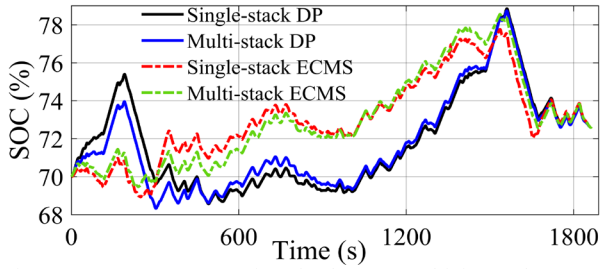

Fig. 14. Battery SOC comparison for the FTP-75 driving cycle.

It does not imply that the SOC must terminate in the initial SOC; rather, the final SOC in the SS system, MS system, and DP must be the same value.

Fig. 15 represents the operation of the SS and MS systems in the safe zone. As can be observed in the MS system (Fig. 15(a)), throughout the whole driving cycle, 97% of the FCs power is in the safe zone, while in the SS system (Fig. 15(b)), this amount decreases to 95.4%.

The MS system works 1.6% more than the SS system in the safe zone. This difference of operation leads to less operating cost for the MS system. Table. IX shows a comprehensive comparison between the SS system and the MS system. Hydrogen cost, degradation cost, and total cost are compared between ECMS and DP. The results show that the MS system is more efficient and economical than the SS system.

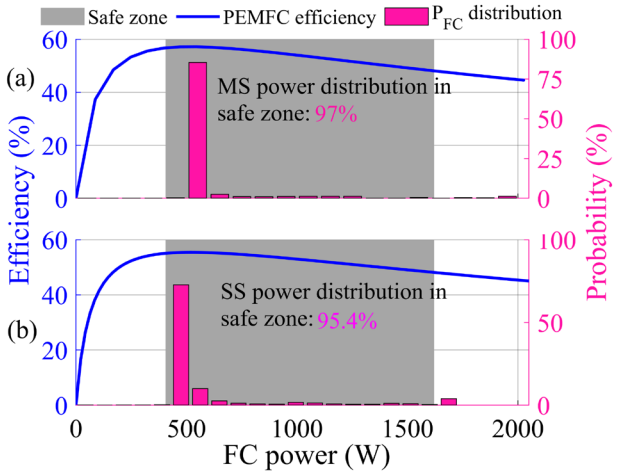

Fig. 15. FC operating in the safe zone for the FTP-75 driving cycle: (a) MS; (b) SS.

TABLE IX
OPERATING COSTS COMPARISON

Driving cycle	WLTC-class3				FTP-75			
EMS	DP		ECMS		DP		ECMS	
Configuration	SS	MS	SS	MS	SS	MS	SS	MS
H_2 cost (Cent)	5.860	5.673	6.400	6.153	6.716	6.514	7.040	6.850
Degradation cost (Cent)	0.011	0.006	0.046	0.010	0.019	0.012	0.074	0.051
Total cost (Cent)	5.870	5.680	6.445	6.163	6.735	6.530	7.114	6.900
	MS 3.2% less than SS		MS 4.4% less than SS		MS 3.0% less than SS		MS 3.0% less than SS	

V. CONCLUSION

This paper aims to compare the operating costs between the SS and the MSFC-HEV. The considered SSFC-HEV in this study is composed of a 2000-W Horizon FC, while the MS one utilizes four 500-W Horizon FCs. Both configurations utilize a battery pack as an ESS. The operating cost consists of hydrogen consumption and FC degradation costs. Indeed, the main objective of this optimization problem is to decide on a suitable FC power signal, as the control variable, to reach the minimum operating cost. To do so, this paper puts forward a hierarchical EMS for the MS system, and the obtained results are compared with those from DP, which is a well-accepted benchmark in this line of work. In the MS system, a rule-based strategy is used in the first layer of the EMS to determine the number of FCs that should participate in the optimization problem of the second layer, where ECMS is responsible for power distribution. The results of this study illustrate that the hydrogen consumption, degradation, and total costs of the MS system are lower than the SS system. Therefore, in terms of operating cost, the MS system can be a suitable choice for an FC-HEV.

REFERENCES

[1] X. Liu, K. Reddi, A. Elgowainy, H. Lohse-Busch, M. Wang, and N. Rustagi, "Comparison of well-to-wheels energy use and emissions of a hydrogen fuel cell electric vehicle relative to a conventional gasoline-powered internal combustion engine vehicle," *Int. J. Hydrogen Energy*, vol. 45, no. 1, pp. 972–983, 2020, doi: 10.1016/j.ijhydene.2019.10.192.

[2] E. Ogungbemi, T. Wilberforce, O. Ijaodola, J. Thompson, and A. G. Olabi, "Selection of proton exchange membrane fuel cell for transportation," *Int. J. Hydrogen Energy*, vol. 46, no. 59, pp. 30625–30640, 2021, doi: https://doi.org/10.1016/j.ijhydene.2020.06.147.

[3] S. Satyapal, "2017 Annual progress report: DOE hydrogen and fuel cells program," 2018.

[4] A. Jacome, D. Hissel, V. Heiries, M. Gerard, and S. Rosini, "Prognostic methods for proton exchange membrane fuel cell under automotive load cycling: A review," *IET Electr. Syst. Transp.*, vol. 10, no. 4, pp. 369–375, 2020, doi: 10.1049/iet-est.2020.0045.

[5] N. Marx, L. Boulon, F. Gustin, D. Hissel, and K. Agbossou, "A review of multi-stack and modular fuel cell systems: Interests, application areas and on-going research activities," *Int. J. Hydrogen Energy*, vol. 39, no. 23, pp. 12101–12111, 2014, doi: 10.1016/j.ijhydene.2014.05.187.

[6] T. Wang, Q. Li, L. Yin, W. Chen, E. Breaz, and F. Gao, "Hierarchical Power Allocation Method Based on Online Extremum Seeking Algorithm for Dual-PEMFC/Battery Hybrid Locomotive," *IEEE Trans. Veh. Technol.*, vol. 70, no. 6, pp. 5679–5692, 2021, doi: 10.1109/TVT.2021.3078752.

[7] J. Zhou, J. Liu, Y. Xue, and Y. Liao, "Total travel costs minimization strategy of a dual-stack fuel cell logistics truck enhanced with artificial potential field and deep reinforcement learning," *Energy*, vol. 239, p. 121866, 2022, doi: 10.1016/j.energy.2021.121866.

[8] Y. Yan, Q. Li, W. Chen, W. Huang, and J. Liu, "Hierarchical management control based on equivalent fitting circle and equivalent energy consumption method for multiple fuel cells hybrid power system," *IEEE Trans. Ind. Electron.*, vol. 67, no. 4, pp. 2786–2797, 2020, doi: 10.1109/TIE.2019.2908615.

[9] A. Khalatbarisoltani, M. Kandidayeni, L. Boulon, and X. Hu, "Power Allocation Strategy based on Decentralized Convex Optimization in Modular Fuel Cell Systems for Vehicular Applications," *IEEE Trans. Veh. Technol.*, vol. 9545, no. c, pp. 1–1, 2020, doi: 10.1109/tvt.2020.3028089.

[10] C. Zhang, T. Zeng, Q. Wu, C. Deng, S. H. Chan, and Z. Liu, "Improved efficiency maximization strategy for vehicular dual-stack fuel cell system considering load state of sub-stacks through predictive soft-loading," *Renew. Energy*, vol. 179, pp. 929–944, 2021, doi: 10.1016/j.renene.2021.07.090.

[11] S. Zhou, G. Zhang, L. Fan, J. Gao, and F. Pei, "Scenario-oriented stacks allocation optimization for multi-stack fuel cell systems," *Appl. Energy*, vol. 308, no. October 2021, p. 118328, 2022, doi: 10.1016/j.apenergy.2021.118328.

[12] X. Li, Z. Shang, F. Peng, L. Li, Y. Zhao, and Z. Liu, "Increment-oriented online power distribution strategy for multi-stack proton exchange membrane fuel cell systems aimed at collaborative performance enhancement," *J. Power Sources*, vol. 512, no. August, p. 230512, 2021, doi: 10.1016/j.jpowsour.2021.230512.

[13] J. Snoussi, S. B. Elghali, M. Benbouzid, and M. F. Mimouni, "Optimal Sizing of Energy Storage Systems Using Frequency-Separation-Based Energy Management for Fuel Cell Hybrid Electric Vehicles," *IEEE Trans. Veh. Technol.*, vol. 67, no. 10, pp. 9337–9346, 2018, doi: 10.1109/TVT.2018.2863185.

[14] N. Mebarki, T. Rekioua, Z. Mokrani, D. Rekioua, and S. Bacha, "PEM fuel cell/ battery storage system supplying electric vehicle," *Int. J. Hydrogen Energy*, vol. 41, no. 45, pp. 20993–21005, 2016, doi: 10.1016/j.ijhydene.2016.05.208.

[15] S. Zendegan, A. Ferrara, S. Jakubek, and C. Hametner, "Predictive Battery State of Charge Reference Generation Using Basic Route Information for Optimal Energy Management of Heavy-Duty Fuel

Cell Vehicles," *IEEE Trans. Veh. Technol.*, p. 1, 2021, doi: 10.1109/TVT.2021.3121129.

[16] D. D. Tran, M. Vafaeipour, M. El Baghdadi, R. Barrero, J. Van Mierlo, and O. Hegazy, "Thorough state-of-the-art analysis of electric and hybrid vehicle powertrains: Topologies and integrated energy management strategies," *Renew. Sustain. Energy Rev.*, vol. 119, p. 109596, 2020, doi: 10.1016/j.rser.2019.109596.

[17] Y. Huang *et al.*, "A review of power management strategies and component sizing methods for hybrid vehicles," *Renew. Sustain. Energy Rev.*, vol. 96, no. April 2017, pp. 132–144, 2018, doi: 10.1016/j.rser.2018.07.020.

[18] T. Teng, X. Zhang, H. Dong, and Q. Xue, "A comprehensive review of energy management optimization strategies for fuel cell passenger vehicle," *Int. J. Hydrogen Energy*, vol. 45, no. 39, pp. 20293–20303, 2020, doi: 10.1016/j.ijhydene.2019.12.202.

[19] C. Zhang *et al.*, "Real-Time Optimization of Energy Management Strategy for Fuel Cell Vehicles Using Inflated 3D Inception Long Short-Term Memory Network-Based Speed Prediction," *IEEE Trans. Veh. Technol.*, vol. 70, no. 2, pp. 1190–1199, 2021, doi: 10.1109/TVT.2021.3051201.

[20] T. Wang, Q. Li, X. Wang, W. Chen, E. Breaz, and F. Gao, "A Power Allocation Method for Multistack PEMFC System Considering Fuel Cell Performance Consistency," *IEEE Trans. Ind. Appl.*, vol. 56, no. 5, pp. 5340–5351, 2020, doi: 10.1109/TIA.2020.3001254.

[21] A. M. I. Fernandez, M. Kandidayeni, L. Boulon, and H. Chaoui, "An Adaptive State Machine Based Energy Management Strategy for a Multi-Stack Fuel Cell Hybrid Electric Vehicle," *IEEE Trans. Veh. Technol.*, vol. 69, no. 1, pp. 220–234, 2020, doi: 10.1109/TVT.2019.2950558.

[22] T. Wang, Q. Li, L. Yin, and W. Chen, "Hydrogen consumption minimization method based on the online identification for multi-stack PEMFCs system," *Int. J. Hydrogen Energy*, pp. 5074–5081, 2019, doi: 10.1016/j.ijhydene.2018.09.181.

[23] W. Zhang, J. Li, L. Xu, and M. Ouyang, "Optimization for a fuel cell/battery/capacity tram with equivalent consumption minimization strategy," *Energy Convers. Manag.*, vol. 134, pp. 59–69, 2017, doi: 10.1016/j.enconman.2016.11.007.

[24] T. Wang *et al.*, "An optimized energy management strategy for fuel cell hybrid power system based on maximum efficiency range identification," *J. Power Sources*, vol. 445, no. October 2019, 2020, doi: 10.1016/j.jpowsour.2019.227333.

[25] H. Li, A. Ravey, A. N'Diaye, and A. Djerdir, "Online adaptive equivalent consumption minimization strategy for fuel cell hybrid electric vehicle considering power sources degradation," *Energy Convers. Manag.*, vol. 192, no. March, pp. 133–149, 2019, doi: 10.1016/j.enconman.2019.03.090.

[26] H. Li, A. Ravey, A. N'Diaye, and A. Djerdir, "A novel equivalent consumption minimization strategy for hybrid electric vehicle powered by fuel cell, battery and supercapacitor," *J. Power Sources*, vol. 395, no. May, pp. 262–270, 2018, doi: 10.1016/j.jpowsour.2018.05.078.

[27] F. Martel, S. Kelouwani, Y. Dubé, and K. Agbossou, "Optimal economy-based battery degradation management dynamics for fuel-cell plug-in hybrid electric vehicles," *J. Power Sources*, vol. 274, pp. 367–381, 2015, doi: 10.1016/j.jpowsour.2014.10.011.

[28] M. Kandidayeni, A. O. M. Fernandez, A. Khalatbarisoltani, L. Boulon, S. Kelouwani, and H. Chaoui, "An Online Energy Management Strategy for a Fuel Cell/Battery Vehicle Considering the Driving Pattern and Performance Drift Impacts," *IEEE Trans. Veh. Technol.*, vol. 68, no. 12, pp. 11427–11438, 2019, doi: 10.1109/TVT.2019.2936713.

[29] M. Kandidayeni, A. Macias, L. Boulon, and S. Kelouwani, "Investigating the impact of ageing and thermal management of a fuel cell system on energy management strategies," *Appl. Energy*, vol. 274, no. December 2019, p. 115293, 2020, doi: 10.1016/j.apenergy.2020.115293.

[30] "Proton-Exchange Membrane Fuel Cells," in *Fuel Cell Systems Explained*, John Wiley & Sons, Ltd, 2018, pp. 69–133.

[31] M. Kandidayeni, J. P. Trovão, M. Soleymani, and L. Boulon, "Towards health-aware energy management strategies in fuel cell hybrid electric vehicles: A review," *Int. J. Hydrogen Energy*, vol. 7, 2022, doi: 10.1016/j.ijhydene.2022.01.064.

[32] M. Yue, S. Jemei, R. Gouriveau, and N. Zerhouni, "Review on health-conscious energy management strategies for fuel cell hybrid electric vehicles: Degradation models and strategies," *Int. J. Hydrogen Energy*, vol. 44, no. 13, pp. 6844–6861, 2019, doi: 10.1016/j.ijhydene.2019.01.190.

[33] J. Zhao and X. Li, "A review of polymer electrolyte membrane fuel cell durability for vehicular applications: Degradation modes and experimental techniques," *Energy Convers. Manag.*, vol. 199, no. August 2019, p. 112022, 2019, doi: 10.1016/j.enconman.2019.112022.

[34] X. Hu, C. Zou, X. Tang, T. Liu, and L. Hu, "Cost-optimal energy management of hybrid electric vehicles using fuel cell/battery health-aware predictive control," *IEEE Trans. Power Electron.*, vol. 35, no. 1, pp. 382–392, 2020, doi: 10.1109/TPEL.2019.2915675.

[35] Y. Zhou, A. Ravey, and M. C. Péra, "Real-time cost-minimization power-allocating strategy via model predictive control for fuel cell hybrid electric vehicles," *Energy Convers. Manag.*, vol. 229, no. September 2020, 2021, doi: 10.1016/j.enconman.2020.113721.

[36] T. Fletcher, R. Thring, and M. Watkinson, "An Energy Management Strategy to concurrently optimise fuel consumption & PEM fuel cell lifetime in a hybrid vehicle," *Int. J. Hydrogen Energy*, vol. 41, no. 46, pp. 21503–21515, 2016, doi: 10.1016/j.ijhydene.2016.08.157.

[37] H. Chen, P. Pei, and M. Song, "Lifetime prediction and the economic lifetime of proton exchange membrane fuel cells," *Appl. Energy*, vol. 142, pp. 154–163, 2015, doi: 10.1016/j.apenergy.2014.12.062.

[38] Q. Li *et al.*, "A state machine control based on equivalent consumption minimization for fuel cell/ supercapacitor hybrid tramway," *IEEE Trans. Transp. Electrif.*, vol. 5, no. 2, pp. 552–564, 2019, doi: 10.1109/TTE.2019.2915689.

[39] X. Lin, Z. Wang, S. Zeng, and W. Huang, "Real-time optimization strategy by using sequence quadratic programming with multivariate nonlinear regression for a fuel cell electric vehicle," *Int. J. Hydrogen Energy*, vol. 46, no. 24, pp. 1–12, 2021, doi: 10.1016/j.ijhydene.2021.01.125.

[40] A. Rabbani and M. Rokni, "Dynamic characteristics of an automotive fuel cell system for transitory load changes," *Sustain. Energy Technol. Assessments*, vol. 1, no. 1, pp. 34–43, 2013, doi: 10.1016/j.seta.2012.12.003.

[41] K. Ettihir, L. Boulon, and K. Agbossou, "Optimization-based energy management strategy for a fuel cell/battery hybrid power system," *Appl. Energy*, vol. 163, pp. 142–153, 2016, doi: 10.1016/j.apenergy.2015.10.176.

[42] A. Macias, M. Kandidayeni, L. Boulon, and J. P. Trovão, "Fuel cell-supercapacitor topologies benchmark for a three-wheel electric vehicle powertrain," *Energy*, vol. 224, 2021, doi: 10.1016/j.energy.2021.120234.

[43] P. Thounthong, S. Raël, and B. Davat, "Test of a PEM fuel cell with low voltage static converter," *J. Power Sources*, vol. 153, no. 1, pp. 145–150, 2006, doi: 10.1016/j.jpowsour.2005.01.025.

[44] W. Zhou, L. Yang, Y. Cai, and T. Ying, "Dynamic programming for new energy vehicles based on their work modes Part II: Fuel cell electric vehicles," *J. Power Sources*, vol. 407, no. October, pp. 92–104, 2018, doi: 10.1016/j.jpowsour.2018.10.048.

Mohammadreza Moghadari (S'21) received a B.S. degree in Mechanical Engineering at Islamic Azad University Central Tehran Branch in 2015 and finished his master's degree in Automotive Engineering at the Iran University of Science and Technology in 2018. He held the 3rd rank among master's students in Automotive Engineering. His research background consists of PEMFC, water management in PEMFC, gas diffusion layer, and CFD. He started his Ph.D. journey in the Hydrogen Research Institute of the University of Quebec, Trois-Rivières (UQTR), QC, Canada, in 2020. He has published several scientific papers in SCI journals since 2016. In the capacity of a reviewer, he has contributed to several scientific journals. PEMFC, water management in PEMFC, optimal control, prediction, deep neural network, energy management strategy, and fault-tolerant control are among his research interests.

Mohsen Kandidayeni (S'18) was born in Tehran (Iran) in 1989. His educational journey has spanned through different paths. He received the B.S. degree in Mechanical Engineering in 2011, and then did a master's degree in Mechatronics at Arak University (Iran) in 2014. He joined the Hydrogen Research Institute of University of Quebec, Trois-Rivières (UQTR), QC, Canada, in 2016 and received his Ph.D. \degree in Electrical Engineering from this university in 2020. He is currently a postdoctoral researcher in electric-Transport, Energy Storage and Conversion Lab (e-TESC) at Université de Sherbrooke and a research assistant member in Hydrogen Research Institute of UQTR. He was a straight-A student during his Master and Ph.D. programs. Moreover, he has been the recipient of several awards/honors during his educational path, such as a doctoral scholarship from the Fonds de recherche du Québec–Nature et technologies (FRQNT), a postdoctoral scholarship from FRQNT, an excellence student grant from UQTR, and the 3rd prize in Energy Research Challenge from the Quebec Ministry of Energy and Natural Resources. He has been actively involved in conducting research through authoring, coauthoring, and reviewing several papers in different prestigious scientific journals and also participating in various international conferences. His research interests include energy-related topics, such as hybrid electric vehicles, fuel cell systems, energy management, Multiphysics systems, modeling, and control.

Loïc Boulon (M'10, SM'15) received the master's degree in electrical and automatic control engineering from the University of Lille (France), in 2006. Then, he obtained a Ph.D. in electrical engineering from the University of Franche-Comté (France). Since 2010, he is a professor at UQTR (Full Professor since 2016) and he works into the Hydrogen Research Institute (Deputy director since 2019). His work deals with modeling, control and energy management of multiphysics systems. His research interests include hybrid electric vehicles, energy and power sources (fuel cell systems, batteries, and ultracapacitors). He has published more than 120 scientific papers in peer-reviewed international journals and international conferences and given over 35 invited conferences all over the world. In 2015, Loïc Boulon was general chair of the IEEE-Vehicular Power and Propulsion Conference in Montréal (QC, Canada). Prof. Loïc Boulon is now VP-Motor Vehicles of the IEEE Vehicular Technology Society and he found the "International Summer School on Energetic Efficiency of Connected Vehicles" and the "IEEE VTS Motor Vehicle Challenge". He is the holder of the Canada Research Chair in Energy Sources for the Vehicles of the future.

Hicham Chaoui (S'01-M'12-SM'13) received the Ph.D. degree in electrical engineering (with honors) from the University of Quebec, Trois-Rivières, QC, Canada, in 2011. His career has spanned both academia and industry in the field of control and energy systems. From 2007 to 2014, he held various engineering and management positions in the Canadian industry. He is currently an Associate Professor with Texas Tech University, TX, USA, and also with Carleton University, Ottawa, ON, Canada. His research interests include adaptive and nonlinear control theory, intelligent control, robotics, electric motor drives, and energy conversion and storage systems. His scholarly work has resulted in over 150 journal and conference publications. Dr. Chaoui is a senior member of IEEE and a registered professional engineer in the province of Ontario. He is also an Associate Editor of IEEE Transactions on Power Electronics and several other IEEE journals. He was the recipient of the Best Thesis Award, the Governor General of Canada Gold Medal Award, the Carleton's Research Excellence Award, the Early Researcher Award from the Ministry of Colleges and Universities, and the Top Editor Recognition from IEEE Vehicular Technology Society.

.